Molecular Orbital Calculations. EHMO calculations were performed on an CDC Cyber 7600 using the ICON subroutine and previously published atomic parameters. Variations in the W–W bond distances of $W_2(\mu\text{-}CH)_2H_4$ and $W_2(\mu\text{-}CH)_2(OH)_4$ caused a smooth decrease in W–W overlap with increasing internuclear distance.

Fenske–Hall MO calculations were performed on a VAX/1170 computer system. Atomic basis functions for Ta(I), W(I), and Re(I) were calculated by Herman–Skillman atomic calculations according to the method of Bursten, Fenske, and Jensen[27] using fixed 6s and 6p exponents and contracted double-ζ representations for the W 5d AO's. Calculations were converged to a population agreement of 0.001. Metal basis functions were derived by using 6s exponents fixed at 1.8 and 6p exponents of 1.6, 1.8, and 2.0 for Ta, W, and Re, respectively. A 1s exponent of 1.16 was used for the H atom. The skeletal coordinates used in the $M_2(\mu\text{-}CH)_2(CH_3)_4$ models of the Ta, W, and Re derivatives were identical with those listed in Table V and the four terminal methyl groups were oriented to retain D_{2h} symmetry.

Acknowledgment. D.L.L. acknowledges support by the U.S. Department of Energy (Division of Chemical Sciences, Office of Basic Energy Sciences, Office of Energy Research, DE-AC02-80ER10746), the National Science Foundation (CHE8519560), and the Materials Characterization Program, University of Arizona. The work at Indiana University was supported by the National Science Foundation and, in part, by the donors of the Petroleum Research Fund, administered by the American Chemical Society.

Appendix

W–H distances of 1.73 Å and H–W–H angles between 122 and 123° were used in all $W_2(\mu\text{-}CH)_2H_4$ EHMO models. W–O distances of 1.85 Å and W–O–H angles of 159° were used in all $W_2(\mu\text{-}CH)_2(OH)_4$ model calculations.

Distances and angles for the $M_2(\mu\text{-}CH)_2$ unit used in Ta, W, and Re model compounds are listed in Table IV. Representative examples of atomic coordinates for CH_3- and OH-substituted model compounds used in FHMO calculations are also listed in Table V.

Registry No. $W(\mu\text{-}CSiMe_3)_2(O\text{-}i\text{-}Pr)_4$, 96930-67-5; $W2(\mu\text{-}CSiMe_3)_2(CH_2SiMe_3)_4$, 107201-08-1; $Ta(\mu\text{-}CSiMe_3)_2(CH_2SiMe_3)_4$, 107201-09-2; *syn*-$W2(\mu\text{-}CSiMe_3)_2(CH_2SiMe_3)_2(O\text{-}t\text{-}Bu)_2$, 103238-36-4; *anti*-$W2(\mu\text{-}CSiMe_3)_2(CH_2SiMe_3)_2(O\text{-}t\text{-}Bu)_2$, 103303-26-0; $W2(\mu\text{-}CH)_2H_4$, 107201-10-5; $Ta_2(m\text{-}CH)_2(CH_3)_4$, 107201-11-6; $W2(\mu\text{-}CH)_2(CH_3)_4$, 107201-12-7; $Re_2(\mu\text{-}CH)_2(CH_3)_4$, 107201-13-8; $W2(\mu\text{-}CH)_2(OH)_4$, 107201-14-9.

Preparation, Structure, and Bonding of $Mo_2(OCH_2CMe_3)_6(\mu\text{-}\eta^1,\eta^2\text{-}NCNMe_2)$

Malcolm H. Chisholm,* John C. Huffman, and Nancy S. Marchant

Department of Chemistry and Molecular Structure Center, Indiana University, Bloomington, Indiana 47405

Received October 17, 1986

Hydrocarbon solutions of $Mo_2(OCH_2\text{-}t\text{-}Bu)_6(M{\equiv}M)$ and R_2NCN (R = Me, Et) react to give a compound of formula $Mo_2(OCH_2\text{-}t\text{-}Bu)_6(\mu\text{-}R_2NCN)$. A single-crystal X-ray diffraction study shows that cyanamide bridges the two molybdenum atoms parallel to the M–M vector. Pertinent bond distances are Mo—Mo = 2.449 (1) Å, C≡N = 1.333 (4) Å, Mo—O (terminal) = 1.91 (average) Å, Mo_1–C = 2.014 (4) Å, and Mo_2–N = 2.134 (3) Å. ^1H NMR studies show the molecule is fluxional at room temperature, involving a turnstile-type motion of three terminal alkoxide ligands. The nature of bonding of the cyanamide ligand to the dimetal center has been investigated by Fenske–Hall calculations on the model system $Mo_2(OH)_6(\mu\text{-}H_2NCN)$. Extensive rehybridization of H_2NCN occurs upon interaction with the dimetal center allowing the cyanamide to act as a donor to both metals. Reduction of the H_2NCN in this compound takes place via back-bonding into the a′ π^* orbital of cyanamide. The reduction of the H_2NCN is suggestive of a model for the reaction pathway of RCN with $W_2(O\text{-}t\text{-}Bu)_6$ leading to carbyne and nitride formation.

Introduction

Prior work has shown $W_2(O\text{-}t\text{-}Bu)_6$ reacts with nitriles to give cleavage of the W≡W and C≡N bond in a metathesis-like manner (eq 1).[1] Similarly, alkynes (though

$$W_2(O\text{-}t\text{-}Bu)_6 + RC{\equiv}N \xrightarrow[\text{alkanes}]{20\ ^\circ C} (t\text{-}BuO)_3W{\equiv}CR + (t\text{-}BuO)_3W{\equiv}N \quad (1)$$

not ethyne) react with $W_2(O\text{-}t\text{-}Bu)_6$ to give alkylidynes $(t\text{-}BuO)_3W{\equiv}CR$.[1,2] Schrock and co-workers have used this metathesis of W≡W and C≡C bonds in the preparation of an extensive class of $(t\text{-}BuO)_3W{\equiv}CR$ compounds which are active toward alkyne metathesis.[3-5] By contrast nitriles and $Mo_2(O\text{-}t\text{-}Bu)_6$ fail to react under similar conditions. Indeed while other N-donor ligands, L, such as pyridine and dimethylamine, reversibly form adducts of formula $Mo_2(OR)_6L_2$ (R = *i*-Pr or CH_2CMe_3 = Np),[6,7] nitriles show little affinity to the dimolybdenum center and may be used as solvents. However, dimethylcyanamide, Me_2NCN, was shown by Kelly[8] to form 1:1 adducts with $Mo_2(O\text{-}t\text{-}Bu)_6$ and $Mo_2(O\text{-}i\text{-}Pr)_6$ and subsequently was found[9] to undergo the metathesis reaction 1 with $W_2(O\text{-}t\text{-}Bu)_6$. The 1:1 adducts between $Mo_2(OR)_6$ compounds and $Me_2NC{\equiv}N$ became of further interest to us as possible models for intermediates in the metathesis of W≡W and C≡N bonds. In the earlier work of Chisholm and Kelly, crystals suitable for X-ray studies were not obtained for $Mo_2(OR)_6(Me_2NCN)$ compounds. We report here the synthesis and

(1) Schrock, R. R.; Listemann, M. L.; Sturgeoff, L. G. *J. Am. Chem. Soc.* **1982**, *104*, 4291.
(2) Listemann, M. L.; Schrock, R. R. *Organometallics* **1985**, *4*, 74.
(3) Schrock, R. R. *ACS Symp. Ser.* **1983**, *No. 221*, 369.
(4) Wengrovius, J. H.; Sancho, J.; Schrock, R. R. *J. Am. Chem. Soc.* **1981**, *103*, 3932.
(5) Sancho, J.; Schrock, R. R. *J. Mol. Catal.* **1982**, *15*, 75.
(6) Chisholm, M. H.; Cotton, F. A.; Extine, M. W.; Reichert, W. W. *J. Am. Chem. Soc.* **1978**, *100*, 153.
(7) Chisholm, M. H. *Polyhedron* **1983**, 2, 681.
(8) Chisholm, M. H.; Kelly, R. L. *Inorg. Chem.* **1979**, *18*, 2321.
(9) Chisholm, M. H.; Huffman, J. C.; Marchant, N. S. *J. Am. Chem. Soc.* **1983**, *105*, 6162.

0276-7333/87/2306-1073$01.50/0

Table I. Atomic Positional Parameters for the $Mo_2(ONp)_6(Me_2NCN)$ Molecule

atom	10^4x	10^4y	10^4z	$10B_{iso}$, Å^2
Mo(1)	2908.4 (2)	999.2 (3)	1284.9 (3)	17
Mo(2)	1862.7 (1)	1773.3 (3)	1353.9 (3)	15
N(3)	2039 (1)	725 (3)	−136 (3)	19
C(4)	2479 (2)	186 (3)	−541 (3)	20
N(5)	2342 (2)	−409 (3)	−1692 (3)	27
C(6)	1657 (2)	−540 (4)	−2702 (4)	39
C(7)	2890 (3)	−922 (4)	−1996 (4)	37
O(8)	2991 (1)	−276 (2)	2623 (2)	25
C(9)	3088 (2)	−1442 (4)	2381 (4)	29
C(10)	3471 (2)	−2005 (3)	3675 (4)	25
C(11)	4227 (2)	−1199 (4)	4221 (5)	39
C(12)	3049 (2)	−2134 (4)	4756 (4)	36
C(13)	3551 (3)	−3226 (4)	3346 (4)	39
O(14)	3656 (1)	2384 (2)	1051 (2)	23
C(15)	4096 (2)	2485 (4)	104 (4)	26
C(16)	4862 (2)	2404 (4)	803 (4)	28
C(17)	5217 (2)	3412 (4)	1837 (5)	43
C(18)	5277 (2)	2538 (4)	−333 (5)	39
C(19)	4854 (2)	1166 (4)	1504 (5)	41
O(20)	2759 (1)	1984 (2)	2875 (2)	19
C(21)	3161 (2)	3066 (3)	3635 (4)	21
C(22)	3470 (2)	2757 (3)	5116 (4)	23
C(23)	3914 (2)	3939 (4)	5817 (4)	33
C(24)	3951 (3)	1875 (4)	5197 (5)	43
C(25)	2859 (2)	2191 (4)	5802 (4)	37
O(26)	1626 (1)	2747 (2)	2607 (2)	20
C(27)	947 (2)	3044 (3)	2194 (4)	23
C(28)	788 (2)	3665 (3)	3315 (4)	25
C(29)	1351 (2)	4840 (4)	3689 (5)	35
C(30)	42 (2)	3935 (4)	2758 (5)	38
C(31)	776 (2)	2827 (4)	4554 (5)	40
O(32)	1050 (1)	534 (2)	1449 (2)	23
C(33)	803 (2)	−711 (3)	1092 (4)	26
C(34)	489 (2)	−1438 (3)	2229 (4)	24
C(35)	−133 (2)	−946 (4)	2401 (4)	33
C(36)	1076 (3)	−1333 (5)	3560 (5)	47
C(37)	215 (2)	−2752 (4)	1791 (5)	35
O(38)	1739 (1)	2974 (2)	−7 (2)	20
C(39)	2022 (2)	3353 (3)	−1172 (4)	26
C(40)	2288 (2)	4721 (3)	−1200 (4)	23
C(41)	2635 (3)	5080 (4)	−2403 (5)	39
C(42)	2847 (3)	5117 (5)	114 (5)	51
C(43)	1661 (3)	5298 (4)	−1378 (6)	54

full structural characterization of one such compound, namely, for R = Np, together with an examination of its dynamic solution behavior and a study of its bonding as determined from a MO calculation employing the method of Fenske and Hall.[10] A preliminary report of the structure has appeared.[9]

Results and Discussion

Syntheses of $Mo_2(ONp)_6(R_2NCN)$ Compounds. $Mo_2(ONp)_6$ reacts with R_2NCN (R = Me, Et) in hydrocarbon solutions virtually instantaneously to give deep red-purple solutions. Deep purple crystals, $Mo_2(ONp)_6(R_2NCN)$, can be isolated from concentrated hexane solutions. These are analogues of $Mo_2(OR)_6(Me_2NCN)$ compounds previously prepared for R = *t*-Bu and *i*-Pr.

Solid-State and Molecular Structure of $Mo_2(ONp)_6(Me_2NCN)$. Figure 1 shows an ORTEP drawing of the molecular structure of $Mo_2(ONp)_6(\mu\text{-}Me_2NCN)$ found in the solid state. Atomic positional parameters are given in Table I, and pertinent bond lengths and bond angles are given in Tables II and III, respectively. There is one virtual mirror plane within the molecule containing the Me_2NCN ligand that is parallel with the M–M vector. The ligand is rigorously planar with a NCN angle of 127°. The C–N distance has lengthened 0.17 Å from the value in free cyanamide, 1.16 Å,[11] to 1.333 (4) Å while the Me_2NCN bond has shortened and is now similar to the other C–N bond length, 1.324 (4) Å. The amide N lone pair is now donating into a π system within the R_2NCN ligand.

The bond lengths and angles of $Mo_2(ONp)_6(\mu\text{-}Me_2NCN)$ (I) can be compared to those found for $Cp_2Mo_2(CO)_4(\mu\text{-}Me_2NCN)$ (II).[11] Although both of the Mo starting com-

Table II. Pertinent Bond Distances (Å) in $Mo_2(OCH_2\text{-}t\text{-}Bu)_6(\mu\text{-}Me_2NCN)$

A	B	dist	A	B	dist
Mo(1)	Mo(2)	2.449 (1)	O(8)	C(9)	1.433 (4)
Mo(1)	O(8)	1.908 (2)	O(14)	C(15)	1.426 (4)
Mo(1)	O(14)	1.918 (2)	O(20)	C(21)	1.445 (4)
Mo(1)	O(20)	2.146 (2)	O(26)	C(27)	1.411 (4)
Mo(1)	N(3)	1.908 (3)	O(32)	C(33)	1.422 (4)
Mo(1)	C(4)	2.014 (4)	O(38)	C(39)	1.418 (4)
Mo(2)	O(20)	1.999 (2)	N(3)	C(4)	1.333 (4)
Mo(2)	O(26)	1.954 (2)	N(5)	C(4)	1.324 (4)
Mo(2)	O(32)	1.872 (2)	N(5)	C(6)	1.451 (5)
Mo(2)	O(38)	1.870 (2)	N(5)	C(7)	1.451 (5)
Mo(2)	N(3)	2.134 (3)			

Table III. Pertinent Bond Angles (Å) for $Mo_2(OCH_2\text{-}t\text{-}Bu)_6(\mu\text{-}Me_2NCN)$

A	B	C	angle
Mo(2)	Mo(1)	O(8)	108.7 (1)
Mo(2)	Mo(1)	O(14)	106.6 (1)
Mo(2)	Mo(1)	O(20)	51.1 (1)
Mo(2)	Mo(1)	N(3)	57.1 (1)
Mo(2)	Mo(1)	C(4)	96.7 (1)
O(8)	Mo(1)	O(14)	126.9 (1)
O(8)	Mo(1)	O(20)	85.6 (1)
O(8)	Mo(1)	N(3)	115.7 (1)
O(8)	Mo(1)	C(4)	106.1 (1)
O(14)	Mo(1)	O(20)	86.9 (1)
O(14)	Mo(1)	N(3)	116.6 (1)
O(14)	Mo(1)	C(4)	107.7 (1)
O(20)	Mo(1)	N(3)	108.1 (1)
O(20)	Mo(1)	C(4)	147.6 (1)
N(3)	Mo(1)	C(4)	39.6 (1)
Mo(1)	Mo(2)	O(20)	56.6 (1)
Mo(1)	Mo(2)	O(26)	136.2 (1)
Mo(1)	Mo(2)	O(32)	112.8 (1)
Mo(1)	Mo(2)	O(38)	109.7 (1)
Mo(1)	Mo(2)	N(3)	48.6 (1)
O(20)	Mo(2)	O(26)	79.6 (1)
O(20)	Mo(2)	O(32)	120.5 (1)
O(20)	Mo(2)	O(38)	121.1 (1)
O(20)	Mo(2)	N(3)	105.2 (1)
O(26)	Mo(2)	O(32)	90.4 (1)
O(26)	Mo(2)	O(38)	89.3 (1)
O(26)	Mo(2)	N(3)	175.2 (1)
O(32)	Mo(2)	O(38)	117.2 (1)
O(32)	Mo(2)	N(3)	87.6 (1)
O(38)	Mo(2)	N(3)	87.7 (1)
Mo(1)	O(8)	C(9)	125.1 (2)
Mo(1)	O(14)	C(15)	125.6 (2)
Mo(1)	O(20)	Mo(2)	72.3 (1)
Mo(1)	O(20)	C(21)	135.2 (2)
Mo(2)	O(20)	C(21)	128.6 (2)
Mo(2)	O(26)	C(27)	117.0 (2)
Mo(2)	O(32)	C(33)	135.8 (2)
Mo(2)	O(38)	C(39)	134.3 (2)
Mo(1)	N(3)	Mo(2)	74.3 (1)
Mo(1)	N(3)	C(4)	74.5 (2)
Mo(2)	N(3)	C(4)	148.8 (2)
C(4)	N(5)	C(6)	121.8 (3)
C(4)	N(5)	C(7)	120.2 (3)
C(6)	N(5)	C(7)	117.9 (3)
Mo(1)	C(4)	N(3)	65.9 (2)
Mo(1)	C(4)	N(5)	167.0 (3)
N(3)	C(4)	N(5)	127.1 (3)

(10) Fenske, R.; Hall, M. B. *Inorg. Chem.* **1972**, *71*, 768.

(11) Chisholm, M. H.; Cotton, F. A.; Extine, M. W.; Rankel, L. A. *J. Am. Chem. Soc.* **1978**, *100*, 802.

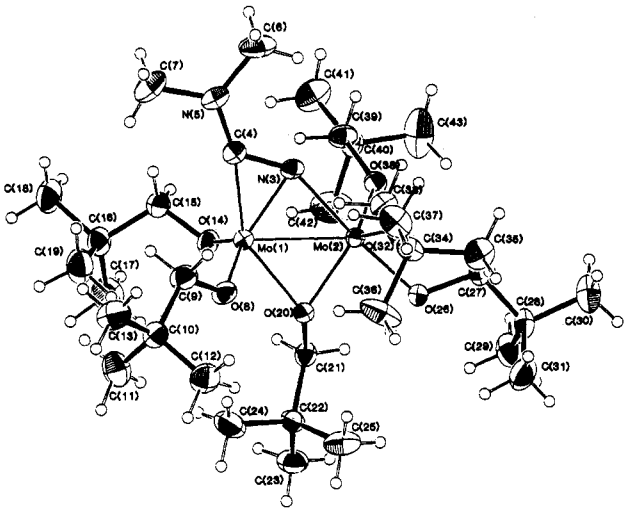

Figure 1. An ORTEP view of the $Mo_2(ONp)_6(\mu\text{-}Me_2NCN)$ molecule giving the atom numbering scheme used in Table II and III.

Table IV. Summary of Crystal Data

empirical formula	$Mo_2O_6N_2C_{33}H_{72}$
color of cryst	red
crystal dimens, mm	0.23 × 0.20 × 0.20
space group	$P\bar{1}$
cell dimens	
T, °C	−120
a, Å	19.738 (6)
b, Å	11.390 (2)
c, Å	10.112 (2)
α, deg	85.42 (1)
β, deg	104.69 (1)
γ, deg	104.20 (1)
Z (molecules/cell)	2
V, Å^3	2131.55
D(calcd), g/cm^3	1.232
wavelength, Å	0.710 69
mol wt	784.82
linear abs coeff, cm^{-1}	6.135
detector to sample dist	22.5
sample to source dist	23.5
takeoff angle	2.0
av ω scan width at half-height	0.25
scan speed, deg/min	40
scan width, deg + dispersion	2.0
individual bkgd, s	4
aperture size, mm	3.0 × 4.0 mm
2θ range, deg	6–45
total no. of reflctns collected	8206
no. of unique intensities	5548
no. with $F > 0.0$	5211
no. with $F > \sigma(F)$	5037
no. with $F > 2.33\sigma(F)$	4771
$R(F)$	0.0313
$R_w(F)$	0.0323
goodness of fit for the last cycle	0.728
max δ/σ for last cycle	0.05

pounds are considered to have M≡M bonds, the two compounds show different affinities for Me_2NCN. In II the C_2NCN unit is also planar but lies at a 42° dihedral angle with respect to the M–M axis. This is due to steric repulsions involving the Cp and Me_2NCN ligands. Also, Me_2NCN binds to $Mo_2(ONp)_6$ more strongly than to $Cp_2Mo_2(CO)_4$. In I relative to II the former C≡N bond is longer (1.333 (4) Å vs. 1.236 (9) Å), the NCN angle is smaller (127° vs. 135°), and the Mo—C distance is shorter (2.014 (4) Å vs. 2.103 (7) Å).

The terminal alkoxide ligands have comparable bond lengths to those found in other $Mo_2(OR)_6$ compounds, indicating that there is some π donation from the alkoxide to the metal. The trans influence of the R_2NCN ligand can be seen in the lengthening of the trans Mo–O bond to 1.954 (2) Å as compared to the other Mo–OR bonds of 1.87 (Å) (average).

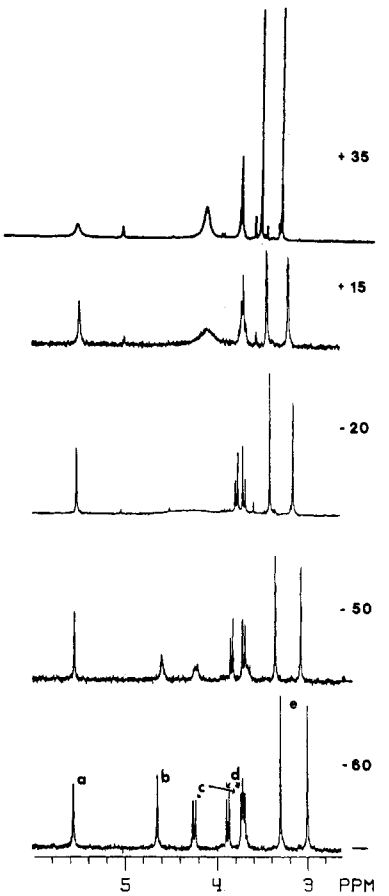

Figure 2. Variable-temperature ^1H NMR spectra of a sample of $Mo_2(ONp)_6(\mu\text{-}Me_2NCN)$ dissolved in toluene-d_8 in the region of the OCH_2CMe_3 (a, b, c, and d) and Me_2NCN (e) protons. Temperatures are shown in degree Celcius.

NMR Studies. $Mo_2(ONp)_6Me_2NCN$ shows interesting temperature-dependent ^1H NMR spectra. The compound has a low-temperature-limiting spectrum that agrees with expectations based on the solid-state structure. The methyl groups of the Me_2NCN ligand are inequivalent due to restricted rotation about the NC–NMe_2 partial double bond. Since the Me_2NCN ligand is oriented parallel with the Mo–Mo bond, the metal atoms are inequivalent and the *N*-methyl groups are proximal and distal. The neopentoxide ligands show four different resonances at −60 °C and are in the integral ratio 2:2:1:1. The two pairs of the ONp ligands have diastereotopic methylene groups giving the AB quartets labeled c and d in Figure 2 for the −60 °C spectrum.

Upon warming to 10 °C two of the methyl resonances, representing three OR groups, broaden and coalesce, while in the methylene region a singlet and an AB quartet (b and c) coalesce. In this temperature region three of the six alkoxide groups are exchanging rapidly while the other three remain frozen out on the NMR time scale. The Me_2N resonances also remain as two sharp singlets indicating that the Me_2NCN ligand is not fluxional at this temperature. This type of behavior can be attributed to rotation of the OR groups (O(26), O(32), and O(38)) about Mo(2) in a turnstile mechanism that does not involve the other three neopentoxide ligands. The activation energy, $\Delta G^{\ddagger} = 12.3 \pm 0.5$ kcal/mol, for this process is estimated from the coalescence temperature.[12]

(12) Sandström, J. *Dynamic NMR Spectroscopy*; Academic: New York, 1982; p 96.

Upon further warming of the sample to 40 °C the AB quartet d coalesces into a broad singlet and the bridging neopentoxide resonance a begins to broaden. Eventually at 60 °C all of the methylene resonances become broad and disappear into the base line, indicating some form of end to end exchange. Above 55 °C the resonances for $Mo_2(O\text{-}Np)_6$ at 4.87 and 1.45 ppm become increasingly prominent in the spectra, indicating that the equilibrium shown in eq 2 is becoming important at higher temperatures. Finally, when the temperature is raised above 75 °C, the compound begins to decompose, perhaps in part due to polymerization of any free Me_2NCN. At no time does a single resonance appear for the methyls of the Me_2NCN ligand. This is in contrast to the fluxional behavior noted for $Mo_2(O\text{-}i\text{-}Pr)_6(Me_2NCN)$ and $Cp_2Mo_2(CO)_4(Me_2NCN)$ at higher temperature,[8,11] indicating that in this case the Me_2NCN ligand is not capable of fluxionality necessary to equilibrate both molybdenum atoms.

$$Mo_2(ONp)_6(Me_2NCN) \rightleftharpoons Mo_2(ONp)_6 + Me_2NCN \quad (2)$$

We have also labeled the central R_2N^*CN carbon with ^{13}C. It was found that Et_2NCN is the easiest cyanamide to label as shown in eq 3. $Mo_2(ONp)_6(Et_2NCN)$ was characterized by IR and NMR spectroscopy and found to be spectroscopically analogous to $Mo_2(ONp)_6(\mu\text{-}Me_2NCN)$. The chemical shift of the central carbon appears at 207 ppm. A CN stretching frequency in the IR spectrum for the Et_2N^*CN labeled compound shifts 30 cm^{-1} from 1552 cm^{-1} in the unlabeled compound to 1522 cm^{-1}.

$$Br^*CN + NEt_3 \rightarrow Et_2N^*CN + BrEt \quad (3)$$

Bonding Considerations. A Fenske–Hall calculation was performed on a model complex $Mo_2(OH)_6(H_2NCN)$. The coordinates for $Mo_2(OH)_6(H_2NCN)$ were idealized to C_s symmetry, but otherwise bond lengths and angles were taken from the crystal structure of $Mo_2(OCH_2\text{-}t\text{-}Bu)_6(Me_2NCN)$. Because of the low symmetry involved in the final compound, a fragment approach will be used to show the interaction of the H_2NCN molecule with the $Mo_2(OH)_6$ fragment.

It is apparent from the crystal structure of I that the cyanamide ligand has been affected by its coordination to the dimetal fragment. It will be important to look first at a brief orbital description of cyanamide itself. Many calculations involving extended Hückel,[13] CNDO,[14] and ab initio[15] methods have been performed on cyanamide and dimethylcyanamide. Much of this theoretical work has focused on the geometric and structural preferences of free cyanamide, though most of those considerations will not be pertinent to the present study. It is agreed that the N–C–N unit is linear and that the amide nitrogen is pyramidal. Nevertheless, there is contribution from the amide lone-pair electrons to the C≡N unit. Due to the involvement of the amide lone-pair, the normally degenerate sets of π and π^* orbitals of the nitrile are split into a four-orbital pattern. By considering the z axis of cyanamide to be parallel to the NCN vector, the a″ π and π^* orbitals interact with the amine lone pair in such a way that a three-orbital pattern is produced to give bonding, nonbonding, and antibonding orbitals very similar to those seen in allyl as shown.

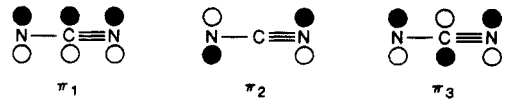

Previous workers have assigned the orbitals as the C≡N π, NR_2 lp, and π^* orbitals on the basis of the orbital densities obtained from extended Hückel calculations using the Wolfsberg–Helmholz and Cusachs approximations.[13] In the present study the Fenske–Hall method shows that more electron density is located on the amide N (40%) than the C and N of the nitrile (29 and 13%, respectively) for the a″ π_1 orbital while for the a″ π_2 orbital more density is located on the nitrile N (45%) than the amide N (25%). These orbital considerations will become more important as the interaction of the cyanamide with the dimetal center is investigated.

Upon coordination to the dimetal fragment the cyanamide bends at the central carbon to give a NCN angle of 127° with concomitant lengthening of the C≡N bond, shortening of the N—C bond, and the amide nitrogen becoming planar. All of these changes serve to enhance the interaction of the amide nitrogen lone pair with the C≡N unit. Now the a″ π and π^* orbitals that are perpendicular to the plane of bending show increased density separation so that the a″ π_1 orbital has 61% of the orbital character located on the amide N. For the a″ π_2 orbital 65% orbital character is located on the nitrile N and 25% on the amide N. This change in the percent orbital character serves to enhance the donor ability of the cyanamide nitrile N atom.

Upon bending at the central carbon the a′ π and π^* orbitals that are parallel with respect to the bending are also affected. Extensive rehybridization takes place via mixing in of additional s and p character contained in the nitrile lone-pair orbital. In this case the nitrile lone-pair mixes with the a′ π bonding orbital so that it has some character at the central carbon and the nitrile lone pair is pointing toward the dimetal center. This mixing raises the energy of the orbital. The a′ π and π^* orbitals are rehybridized so that the orbital density is skewed away from the angle of bending. This lowers the energy of the π^* orbital extensively.

Figure 3 shows the changes in energy and the rehybridization that the cyanamide ligand undergoes upon bending to 127° at the central carbon. In general the effect on the cyanamide is to raise the energy of the a″ π_2 nonbonding orbital and the N lone-pair orbital, while the π^* orbitals are lowered. These changes in energy will enhance the interaction of the cyanamide with the dimetal center.

Because of the low symmetry of the $Mo_2(OH)_6$ fragment, its orbital description is not straight forward. It is advantageous to view the dimetal fragment as the joining together of $Mo(OH)_3$ and $Mo(OH)_4$ fragments. The Mo(1)$(OH)_3$ moiety may be viewed as a d^4 metal fragment having a dative bond from the bridging OH group. The Mo(2)$(OH)_4$ is then counted as a d^2 metal center. The z axes of the $M(OH)_x$ units are pointed toward the cyanamide ligand. As has been discussed at length elsewhere[16] π donation from the alkoxide ligands alters the fragment MO energy ordering of ML_x fragments[17] by raising the energy of the metal-based orbitals.

The important interactions in this case are between the metal-centered molecular orbitals. As shown in Figure 4, three orbitals, mainly metal in character, can be expected to overlap. These orbitals may be viewed as the remnants of the metal–metal triple bond in the unbridged $Mo_2(OR)_6$ species that has been rehybridized due to the reorientation of the alkoxide ligands. The other metal-based orbitals do not interact and come across as nonbonding orbitals

(13) Hanneike, H. F.; Drago, R. S. *J. Am. Chem. Soc.* **1968**, *90*, 5112.
(14) Stafast, H.; Bock, H. *Chem. Ber.* **1974**, *107*, 1882.
(15) Howell, J. M.; Rossi, A. R.; Bissell, R. *Chem. Phys. Lett.* **1976**, *39*, 312.
(16) Blower, P. J.; Chisholm, M. H.; Clark, D. L.; Eichhorn, B. W. *Organometallics* **1986**, *5*, 2125.
(17) Elian, M. E.; Hoffman, R. *Inorg. Chem.* **1975**, *14*, 1058.

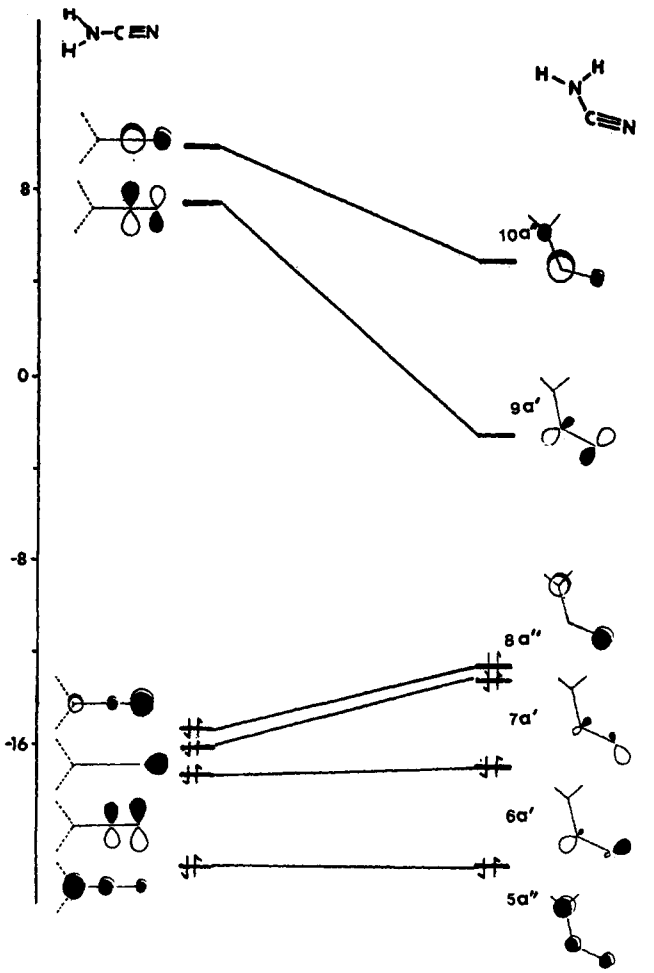

Figure 3. The frontier orbitals of H_2NCN upon bending the NCN angle to 127°.

centered on each respective metal atom. Figure 5 shows a schematic view of the orbitals that are important in the interaction of the $Mo_2(OH)_6$ fragment with the cyanamide ligand. Rehybridization takes place within the π-type orbitals on the metal centers in order to enhance the overlap between the metals, creating a strong π bond in the 2a″ orbital. The nonbonding character of the 4a″ and 3a″ orbitals is also enhanced in this rehybridization of the $M_2(OH)_6$ fragment. In the final $M_2(OH)_6$ fragment the orbital density has been skewed toward the less substituted metal Mo(1), and this metal ultimately shows the most interaction with the cyanamide ligand.

To examine the interaction of the bent H_2NCN ligand with the $M_2(OH)_6$ unit it is convenient to divide the interactions into groups based on the cyanamide orbitals. These groups will consist of the nitrile N lone-pair orbital (7a′), the π and π^* orbitals that are in the plane of bending of the cyanamide ligand (6a′ and 9a′), and the π system that is perpendicular to the plane of bending (5a″, 8a″, and 10a″).

The nitrile lone pair is directed toward the dimetal center, and it shows a very strong σ interaction with the $Mo_2(OH)_6$ orbital 2a′. The latter corresponds to dsp hybrid orbital centered on each metal and is directed toward the nitrile N atom. It should be noted that the rehybridization of the nitrile lone pair upon bending the cyanamide has made it possible to donate electron density from the cyanamide to both metal centers.

The cyanamide 6a′ and 9a′ orbitals correspond to the π and π^* orbitals contained within the plane of bending. The 6a′ interacts with the 4a′ of the $Mo_2(OH)_6$ fragment

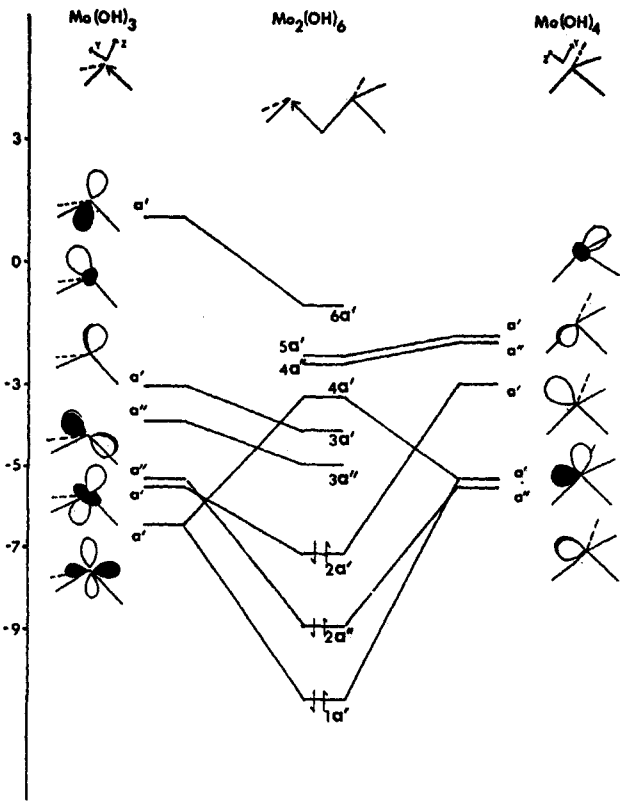

Figure 4. The orbital interaction diagram for $Mo(OH)_3$ and $Mo(OH)_4$ where the $Mo(OH)_4$ has one dative-type alkoxide.

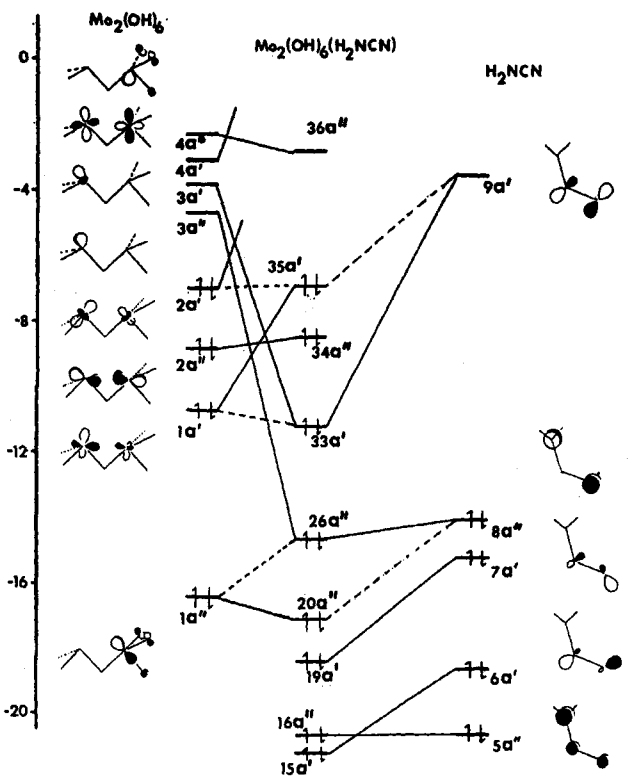

Figure 5. The orbital interaction diagram for $Mo_2(OH)_6$ with H_2NCN.

corresponding to the out-of-phase combination of metal d_{yz} orbitals. This interaction is enhanced by bending at the central carbon on the cyanamide ligand. The 9a′ (π^*) orbital of cyanamide shows more interaction with the dimetal center than 6a′, since it matches the metal-based orbitals energetically and has good overlap with them. The 9a′ interacts with metal-based orbitals to give bonding,

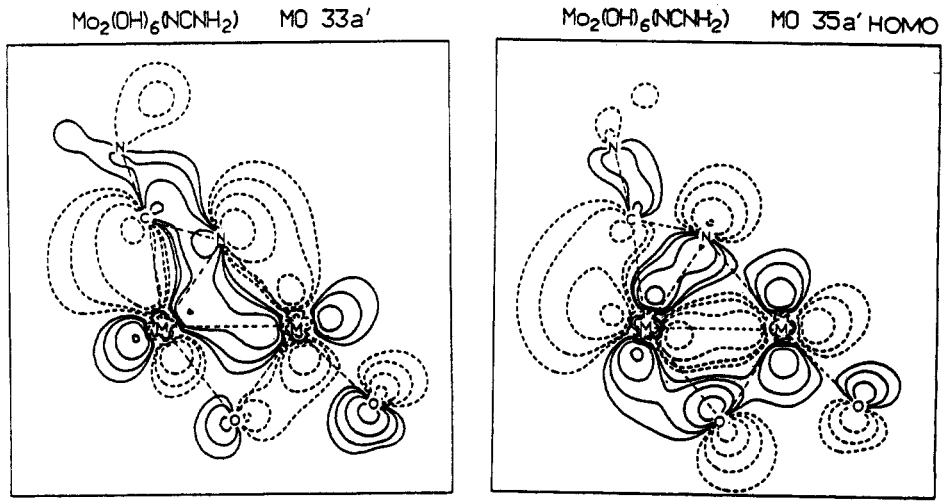

Figure 6. Contour plots of the $Mo_2(OH)_6(\mu\text{-}H_2NCN)$ 33a′ and 35a′ orbitals showing the bonding interaction of the H_2NCN π^* with $Mo_2(OH)_6$. Plots represent a slice taken through the plane containing the $M_2(\mu\text{-}H_2NCN)$ moiety.

nonbonding, and antibonding orbitals. There is mixing of the M–M σ-bonding orbitals and the metal 3a′ orbital which may be viewed as the $d_{x^2-y^2}$ orbital of Mo(1). The interaction with 3a′ produces Mo 33a′ of the composite molecule. Some M–M σ-bond character is present in the 33a′ orbital, though orbital 35a′ contains most of the M–M σ-bond character and is the HOMO of $Mo_2(OH)_6(H_2NCN)$. This can be shown most clearly in Figure 6 by comparing the contour plots for $Mo_2(OH)_6(H_2NCN)$ orbitals 33a′ and 35a′.

Considering now the π system that is perpendicular to the plane of bending at the central carbon, it is noteworthy that the highest (10a″) (not shown in Figure 5 but the antibonding counterpart of 5a″) and lowest (5a″) orbitals of cyanamide do not interact with the dimetal center. Most of the orbital density in 5a″ is located on the amide N atom away from the dimetal center, and, therefore, it is not surprising that it does not show any interaction. The cyanamide orbital 8a″ (π_2) interacts with three $Mo_2(OH)_6$ orbitals 1a″, 3a″, and 4a″. The $Mo_2(OH)_6$ 1a″ orbital is mostly Mo-to-OH π bonding in character while the antibonding counterpart is orbital 4a″. They mix with $Mo_2(OH)_6$ orbital 3a″ to give bonding, nonbonding, and antibonding combinations with the cyanamide 8a″ orbital. Most of the bonding interaction between the cyanamide and the dimetal center comes from the interaction with the $Mo_2(OH)_6$ orbital 3a″ so that the cyanamide is actually π bonding to Mo(1). However, there is some π donation from the cyanamide 8a″ orbital stabilizing the $Mo_2(OH)$ π-bonding orbital (20a″) and π-antibonding character from the cyanamide to Mo_2 in the $Mo_2(OH)_6(H_2NCN)$ orbital 36a″. A simple way to look at this interaction is to say that the cyanamide 2a″ orbital π donates to Mo(2) in $Mo_2(OH)_6(H_2NCN)$ orbital 20a″, π bonds to Mo(1) in $Mo_2(OH)_6(H_2NCN)$ orbital 26a″, and is in a nonbonding interaction with both metals in $Mo_2(OH)_6(H_2NCN)$ orbital 36a″. Figure 7 shows the contour plots of these three orbitals.

To summarize, (1) there is extensive mixing among many molecular orbitals since the molecule is of low symmetry. (2) The HOMO is mainly metal–metal σ bonding in character with some nonbonding contribution from the cyanamide. (3) The LUMO is metal–metal nonbonding with most (53%) of the orbital character centered on Mo(2). (4) Only one π^* orbital (9a′) of cyanamide shows any interaction with the dimetal center and has a high overlap with $Mo_2(OH)_6$. The orbital population (Mulliken population) of the 9a′ orbital after interaction with $Mo_2(OH)_6$ is 1.014 which supports the view that the cyanamide is being reduced by the dimetal center. (5) The interaction of the cyanamide ligand with the dimetal center has been enhanced by bending at the central carbon of the cyanamide ligand.

Table V. Comparison of Mulliken Orbital Populations for $Mo_2(OH)_6(H_2NCN)$ with H_2NCN: Free (A), Linear Coordinated (B), and Bent Coordinated (C)

H_2NCN orbital	A	B	C
5a″ (π^1)	2.00	2.001	2.002
6a′ (π)	2.00	1.799	1.724
7a′ (C≡N 1p)	2.00	1.615	1.596
8a″ (π^2)	2.00	1.809	1.755
9a′ (π^*)		0.843	1.013
10a″ (π^{3*})		0.071	0.088

The enhancement may be shown by comparing the Mulliken populations of the cyanamide ligand orbitals if bending at the central carbon did not occur. Table V shows that less electron density is located in the 9a′ π orbital, which accepts electron density from the dimetal center, if the cyanamide ligand is linear. Within the filled orbitals of cyanamide, which donate electron density to the $(Mo)_2$ unit, the Mulliken population is higher for the linear cyanamide. This demonstrates that the bent cyanamide is also a beter donor toward the dimetal center than a linear cyanamide. Therefore, bending at the central carbon of cyanamide serves to enhance both the donating and accepting abilities of the cyanamide ligand.

Concluding Remarks

We believe it is unreasonable to suppose that cleavage of the C≡N bond in I to give alkylidyne and nitrido molybdenum compounds is hindered by kinetic factors. Rather we propose that this cleavage occurs for reactions involving $W_2(O\text{-}t\text{-}Bu)_6$ but not for $Mo_2(O\text{-}t\text{-}Bu)_6$ because the W_2 center is more reducing.

There are a number of ways that this fact may be quantitatively assessed. For example, in the absence of ligation photoionizations from the M–M π orbitals in $M_2(O\text{-}t\text{-}Bu)_6$ compounds occur at 6.80 and 6.28 eV for M = Mo and W, respectively.[18] Upon complexation with a π-acceptor ligand, X, the compounds $M_2(O\text{-}t\text{-}Bu)_6(\mu\text{-X})$ are formed, where X = CO[19] or C_2H_2.[20] The values of ν(CO)

(18) Kober, E. M.; Lichtenberger, D. L. *J. Am. Chem. Soc.* **1985**, *107*, 7199.

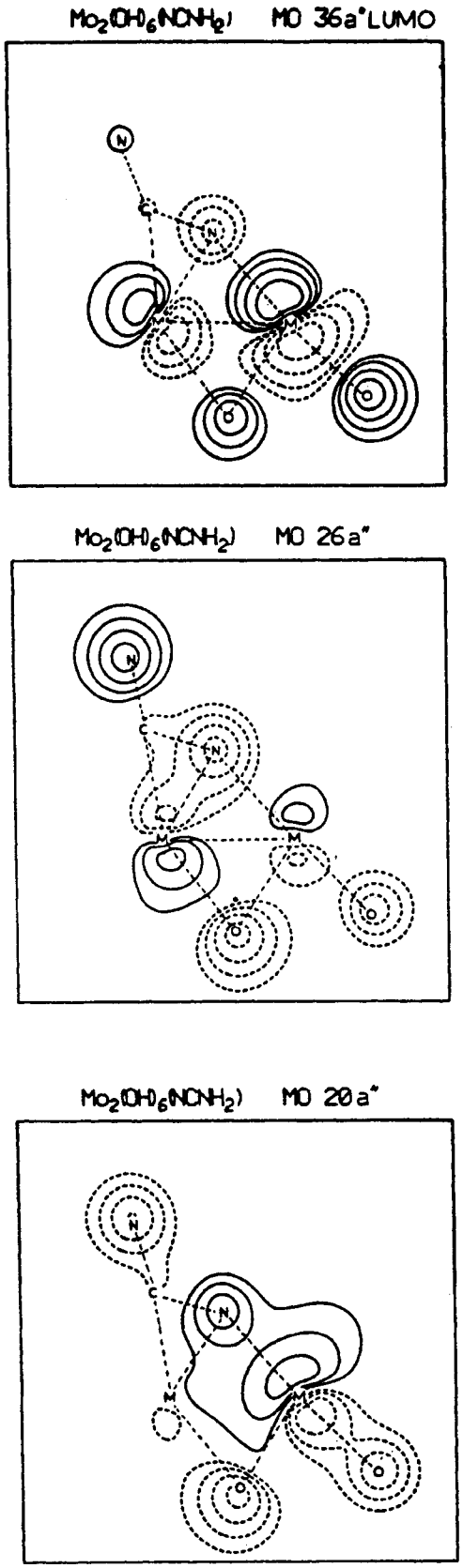

Figure 7. Contour plots of the 20a″, 26a″, and 36a″ of $Mo_2(OH)_6(\mu\text{-}H_2NCN)$ emphasizing the interaction of the a″ π orbital of H_2NCN with $Mo_2(OH)_6$. The plots represent a slice taken just above the plane containing the $M_2(\mu\text{-}H_2NCN)$ moiety.

are at 1670 and 1590 cm^{-1} for M = Mo and W, respectively.[19] The lower value of ν(CO) for M = W is a reflection of greater M-to-CO π^* bonding, and this is seen in the Mulliken populations of the CO 2π MO's as determined by Fenske–Hall calculations.[16] For the $\mu\text{-}C_2H_2$ ligand the magnitude of the $^1J_{C-C}$ provides a measure of C–C bond order reduction and shows an inverse correlation with C–C distance. $^1J_{C-C}$ in the $M_2(O\text{-}t\text{-}Bu)_6(\mu\text{-}C_2H_2)$ compounds are 24 and 11 Hz for M = Mo and W, respectively.[20] For tungsten the $\mu\text{-}C_2H_2$ compound is in equilibrium with the methylidyne complex $(t\text{-}BuO)_3W{\equiv}CH$, but no such equilibrium is present for molybdenum.[20,21]

From the present study we can imagine that enhanced tungsten-to-cyananide π^* bonding will further weaken the C–N bond and strength the W–C and W–N bonds. Reaction 1, which may be viewed as an oxidative cleavage of the $(W{\equiv}W)^{6+}$ center to give two W^{6+}-containing compounds, would then become thermodynamically favored for tungsten. It is, of course, impossible to rule out that the difference in reactivity of the $(M{\equiv}M)^{6+}$ units has a kinetic component, though in our opinion this is not at the crux of the matter.

Finally, it should be noted that the ability of the dialkylamido-substituted cyanides to bind to $Mo_2(OR)_6$ compounds and the relative inertness of alkyl or aryl cyanides (nitriles) can be understood in terms of the participation of the dialkylamido lone pair. As is seen from the calculations, the effect of the latter is to enhance the nucleophilicity of the nitrogen of the C≡N function.

Experimental Section

Reagents and General Techniques. General procedures and the preparation of $Mo_2(OCH_2\text{-}t\text{-}Bu)_6$ have been described.[22] Me_2NCN, Et_2NCN, and $i\text{-}Pr_2NCN$ were purchased from Aldrich, vacuum distilled, and dried over molecular sieves before use. Dry and oxygen-free solvents were used in all preparations, and all manipulations were done under an inert atmosphere (N_2) by using Schlenk and drybox techniques. Elemental analyses were performed by Alfred Bernhart Microanalytisches Laboratorium, West Germany.

^1H NMR spectra were recorded on a Nicolet NT-360 360-MHz and Varian HR-220 spectrometers in dry and oxygen-free toluene-d_8 or benzene-d_6. ^{13}C NMR spectra were recorded on a Nicolet NT-360 or Varian XL-300 spectrometer. The ^{13}C NMR spectrum was obtained for the $\mu\text{-}Et_2NCN$ ligand by using ^{13}C-labeled Et_2N^*CN. Carbon-13-labeled NaCN was purchased from MSD Isotopes and used as described below. All ^1H NMR chemical shifts are in parts per million relative to protio impurities in the solvent. ^{13}C NMR chemical shifts are in parts per million relative to the ipso carbon of toluene-d_8 set at δ 137.5.

Infrared spectra were obtained on a Perkin-Elmer 283 spectrometer as Nujol mulls between CsI plates.

$Et_2N^{13}CN$. $Br^{13}CN$ was prepared from $Na^{13}CN$ according to previously published methods.[23] It should be noted that BrCN is a volatile toxic compound and care should be taken during preparation. Excess Et_3N was added to a hexane suspension of $Br^{13}CN$ and stirred at room temperature for 2 h. The reaction solution was filtered and then fractionally distilled under vacuum to isolate $Et_2N^{13}CN$.

$Mo_2(OCH_2\text{-}t\text{-}Bu)_6(Me_2NCN)$. $Mo_2(ONp)_6$ (0.30 g, 0.419 mmol) was dissolved in toluene (6 mL). Me_2NCN (35 μL) was added via syringe. The solution was stirred at room temperature for 1 h and the solvent removed in vacuo. The remaining purple solid was extracted with hexane and gave deep purple crystals upon cooling to −15 °C: IR (cm^{-1}) 1694 (s), 1422 (s), 1253 (w),

(19) Chisholm, M. H.; Hoffman, D. M.; Huffman, J. C. *Organometallics* **1985**, *4*, 986.

(20) Chisholm, M. H.; Conroy, B. K.; Eichhorn, B. W.; Folting, K.; Hoffman, D. M.; Huffman, J. C.; Marchant, N. S. *Polyhedron*, in press. The formation of $Mo_2(O\text{-}t\text{-}Bu)_6(\mu\text{-}C_2H_2)$ was first noted elsewhere: Strutz, H.; Schrock, R. R. *Organometallics* **1984**, *3*, 1600.

(21) Chisholm, M. H.; Folting, K.; Hoffman, D. M.; Huffman, J. C. *J. Am. Chem. Soc.* **1984**, *106*, 6794.

(22) Chisholm, M. H.; Cotton, F. A.; Murillo, C. A.; Reichert, W. W. *Inorg. Chem.* **1978**, *100*, 153.

(23) Hartman, W. W.; Dreger, E. E. *Organic Synthesis*; Wiley: New York, 1900; Vol. II, p 150.

1212 (w), 1092 (m), 1045 (vs), 1020 (vs), 931 (w), 760 (w), 752 (w), 733 (m), 680 (s), 650 (s), 470 (m), 410 (m). ^{1}H NMR (−60 °C) δ 5.53, 4.58 (s, OCH_2-t-Bu), 4.21, 3.67 (d of an AB quartet, OCH_2-t-Bu), 3.82, 3.69 (d of an AB quartet, OCH_2-t-Bu), 3.32, 3.03 (s, Me_2NCN), 1.46, 1.14, 0.967, 0.870 (s, 1:1:2:2, OCH_2-t-Bu). Anal. Calcd: C, 50.50; H, 9.24; N, 3.57. Found: C, 50.44; H, 9.14; N, 3.46.

Mo_2(OCH_2-t-Bu)$_6$(Et_2NCN). The diethylcyanamide complex was prepared in an analogous manner to that above but employing Et_2NCN: IR (cm^{-1}) 1552 (m), 1256 (w), 1210 (w), 1050 (sh), 1039 (s), 1012 (vs), 930 (w), 840 (w), 756 (m), 720 (m), 673 (m), 637 (m), 465 (m), ν(CN^{13}CN) 1522. ^{1}H NMR (−60 °C) 5.57, 4.64 (s, OCH_2-t-Bu), 4.25, 3.75, 3.86, 3.68 (d of AB quartets, OCH_2-t-Bu), 3.92, 3.55, 1.14 (q, mult, *Et*$_2$NCN), 1.65, 1.49, 0.998, 0.85 (s, 1:1:2:2, OCH$_2$-t-*Bu*). ^{13}C{^{1}H} NMR: δ 207 (Et_2N*C*N). Anal. Calcd: C, 51.72; H, 9.44; N, 3.45. Found: C, 51.47; H, 9.28, N, 3.53.

Computational Data. The model system $Mo_2(OH)_6(H_2NCN)$ was used to investigate the nature of the $M_2(R_2NCN)$ bonding. The coordinates were idealized to C_s symmetry, but otherwise bond lengths and angles were taken from the crystal structure of Mo_2(OCH_2-t-Bu)$_6$(μ-Me_2NCN). Nonempirical Hartree–Fock molecular orbital calculations were performed by H using the self-consistent field Fenske–Hall method (program MEDIEVEL). SCF calculations were performed in the atomic basis on H_2NCN (linear and bent) and $Mo_2(OH)_6$ fragments and on $Mo_2(OH)_6$(μ-H_2NCN). The converged wave functions for the fragments were transformed into appropriate fragment MO bases. Contour plots of the final molecular orbitals were generated via the programs MOPLOT and CONPLOT.

Basis functions for the atoms were generated by a best fit of Herman–Skillman atomic calculations. Contracted double-ζ representations were used for Mo 4d AO's as well as C, O, and N 2p AO's. The basis functions for the metal atoms were derived for a +1 oxidation state with the valence s and p exponents fixed at 1.8 for each of Mo 5s and 5p orbitals. An exponent of 1.16 was used for the H 1s atomic orbital.

Crystallographic Studies. General operating procedures and listings of programs have been previously given.[24] Crystal data are summarized in Table IV.

Data were collected at 165 °C; however, it was not possible to obtain a complete data set at this temperature due to a phase transition. A second data set was taken of the higher temperature phase. It appears the phase transition occurs near −120 °C. In any case there were no evidence of a transition during the present data collection. Attempts to lower the temperature to obtain the low-temperature phase were unsuccessful, with the crystal fracturing upon cooling.

The high-temperature phase was solved by Patterson and Fourier techniques, and all hydrogen atoms were located. Hydrogen thermal parameters were fixed and only their fractional coordinates allowed to vary during refinement. The primary difference is in the relative orientation of the OR groups, although a slight difference is seen in the $NCNMe_2$ ligand.

Acknowledgment. We thank the Department of Energy, Office of Basic Research, Chemical Sciences Division, and the Wrubel Computing Center for financial support and Professor David M. Hoffman for helpful and critical comments.

Registry No. Mo_2(OCH_2-t-Bu)$_6$(Me_2NCN), 86784-87-4; Mo_2(OCH_2-t-Bu)$_6$(Et_2NCN), 100813-13-6; $Mo_2(OH)_6(H_2NCN)$, 106905-66-2; $Et_2N^{13}CN$, 106905-67-3; $Mo_2(ONp)_6$, 62521-24-8; $Br^{13}CN$, 70610-98-9; Et_3N, 121-44-8; Mo, 7439-98-7.

Supplementary Material Available: Tables of anisotropic thermal parameters and complete listings of bond distances and angles (5 pages); listings of F_o and F_c (19 pages). Ordering information is given on any current masthead page.

(24) Chisholm, M. H.; Huffman, J. C.; Folting, K.; Kirkpatrick, C. C. *Inorg. Chem.* **1984**, *23*, 1021.

Synthesis and Structure of a Novel Rhodium(I) Complex, P_3RhP' (P = $P(OPh)_3$, P′ = $PO(OPh)_2^-$): Application of 2D ^{31}P, ^{1}H, ^{13}C, and ^{17}O NMR Spectroscopy

S. Aygen and R. van Eldik*

Institute for Physical Chemistry, University of Frankfurt, Niederurseler Hang, D-6000 Frankfurt/Main 50, FRG

Received October 2, 1986

The structure of a novel rhodium(I) complex, P_3RhP' (1, P = $P(OPh)_3$, P′ = $PO(OPh)_2^-$), was investigated by means of 2D ^{31}P, ^{13}C, ^{1}H, and ^{17}O NMR spectroscopy. The title compound may be prepared either via the reaction of Rh(acac)(CO)$_2$ with excess $P(OPh)_3$ in EtOH or by treating P_4RhClO_4 with KOH in $CHCl_3/C_6H_6$. In both cases a free or coordinated $P(OPh)_3$ ligand is transformed into a diphenyl phosphonate ion, O=$P(OPh)_2^-$, with concurrent loss of phenol. The mechanism of the resulting process may be interpreted as an organometallic variation on the Michaelis–Arbuzov reaction.

Introduction

Irreversible isomerization reactions with alkyl group migration in trialkyl phosphite ($P(OR)_3$) transition-metal complexes have been known for a long time.[1] Ru(P(OCH_3)$_3$)$_5$, for example, isomerizes already at 120 °C via a methyl group shift to form $((H_3CO)_3P)_4Ru(CH_3)P(O)(OCH_3)_2$.[2] Trimethyl phosphite undergoes isomerization at 200 °C to give $H_3CP(O)(OCH_3)_2$.[3] The process is catalyzed by methyl halides in the well-known Michaelis–Arbuzov reaction.[4] This kind of rearrangement or isomerization has hitherto not been observed for $P(OPh)_3$, whereas an

(1) (a) Haines, R. S.; Nolte, C. R. *J. Organomet. Chem.* **1970**, *24*, 725. (b) Haines, R. S.; Du Preez, A. L.; Marais, L. *Ibid.* **1971**, *28*, 405. (c) Neukomm, H.; Werner, H. *Ibid.* **1976**, *108*, C26. (d) Conder, H. L.; Courtney, A. r.; DeMareg, D. *J. Am. Chem. Soc.* **1979**, *101*, 1606. (e) Hawell, J. A. S.; Rowan, A. J. *J. Chem. Soc. Dalton Trans.* **1980**, 1845.

(2) (a) Choi, H. W.; Gaum, R. M.; Muetterties, E. L. *J. Chem. Soc., Chem. Commun.* **1979**, 1085. (b) Van Catledge, F. A.; Ittel, S. D.; Tolman, C. A.; Jesson, J. P. *Ibid.* **1980**, 254. (c) Pomeroy, R. P.; Alex, R. F. *Ibid.* **1980**, 1114. (d) Alex, R. F.; Pomeroy, R. K. *Organometallics* **1982**, *1*, 453.

(3) Marek, V. *Mech. Mol. Migr.* **1969**, *2*, 319.

(4) Kirby, A. S.; Warren, S. G. *Theorectical Organic Chemistry of Phosphorus*: Elsevier: New York, 1967, p 37.

0276-7333/87/2306-1080$01.50/0